Global and Planetary Change 232 (2024) 104336

Contents lists available at ScienceDirect

Global and Planetary Change

journal homepage: www.elsevier.com/locate/gloplacha

Recent summer warming over the western Mediterranean region is unprecedented since medieval times

Ulf Büntgen [a,b,c,*], Frederick Reinig [d], Anne Verstege [e], Alma Piermattei [f,g], Marcel Kunz [d], Paul Krusic [a], Philip Slavin [h], Petr Štěpánek [b], Max Torbenson [d], Edurne Martinez del Castillo [d], Tito Arosio [a], Alexander Kirdyanov [a,i], Clive Oppenheimer [a], Mirek Trnka [b], Audrey Palosse [a], Tatiana Bebchuk [a], J. Julio Camarero [j], Jan Esper [b,d]

[a] Department of Geography, University of Cambridge, Cambridge CB2 3EN, UK
[b] Global Change Research Institute (CzechGlobe), Czech Academy of Sciences, 603 00 Brno, Czech Republic
[c] Department of Geography, Faculty of Science, Masaryk University, 611 37 Brno, Czech Republic
[d] Department of Geography, Johannes Gutenberg University, 55099 Mainz, Germany
[e] Swiss Federal Research Institute (WSL), 8903 Birmensdorf, Switzerland
[f] Department of Agricultural, Forest and Food Sciences, University of Torino, Largo Paolo Braccini, 2, 10095 Grugliasco, TO, Italy
[g] Forest Biometrics Laboratory, Faculty of Forestry, Stefan cel Mare University of Suceava, 720229 Suceava, Romania
[h] Division of History, Heritage and Politics, University of Stirling, Stirling FK9 4LA, UK
[i] Sukachev Institute of Forest SB RAS, Federal Research Center 'Krasnoyarsk Science Center SB RAS', 660036 Krasnoyarsk, Akademgorodok, Russian Federation
[j] Pyreneean Institute of Ecology (IPE), 50059 Zaragoza, Spain

ARTICLE INFO

Editor: Dr. Jed O Kaplan

Keywords:
Anthropogenic warming
Climate change
Human history
Iberian Peninsula
Paleoclimate
Proxy reconstructions
Tree rings
Volcanic eruptions
Wood density

ABSTRACT

Contextualising anthropogenic warming and investigating linkages between past climate variability and human history require high-resolution temperature reconstructions that extend before the period of instrumental measurements. Here, we present maximum latewood density (MXD) measurements of 534 living and relict *Pinus uncinata* trees from undisturbed upper treeline ecotones in the Spanish central Pyrenees. Spanning the period 1119–2020 CE continuously, our new MXD composite chronology correlates significantly with gridded May–September mean temperatures over the western Mediterranean region ($r = 0.76$; $p \leq 0.001$; 1950–2020 CE). Based on an integrative ensemble approach, our reconstruction reveals unprecedented summer warming since 2003 CE. The coldest and warmest reconstructed temperature anomalies are −3.4 (±1.4) °C in 1258 and 2.6 (±2.2) °C in 2017 (relative to 1961–90). Abrupt summer cooling of −1.5 (±1.0) °C was found after 20 large volcanic eruptions since medieval times. Comparison of our summer temperature reconstruction with newly compiled historical evidence from the Iberian Peninsula suggests a lack of military conflict during or following exceptionally hot or cold summers, as well as a general tendency towards less warfare and more stable wheat prices during warmer periods. Our study demonstrates the importance of updating and refining annually resolved and absolutely dated climate reconstructions to place recent trends and extremes of anthropogenic warming in a long-term context of natural temperature variability, and to better understand how past climate and environmental changes affected ecological and societal systems.

1. Introduction

With more than 520 million inhabitants, ample archaeological and historical sources, and a variety of terrestrial and marine ecosystems, the Mediterranean is recognised as a 'global change hot spot' (Giorgi, 2006; Plan Bleu, 2020). At the crossroads of Europe, Asia and Africa, the region has a long history of human migration and cultural exchange (Abulafia, 2011). Much of the Mediterranean basin experienced record-breaking summer warmth in 2022 (Serrano-Notivoli et al., 2023), and climate model projections almost uniformly point to a continuation of warming and drying over much of southern Europe, the Near East and northern Africa (Seager et al., 2014; Fischer and Knutti, 2015; Kelley et al., 2015). An increased frequency and intensity of double jet stream states over Eurasia is likely to accelerate the incidence of summer

* Corresponding author at: Department of Geography, University of Cambridge, Cambridge CB2 3EN, UK.
E-mail address: ulf.buentgen@geog.cam.ac.uk (U. Büntgen).

https://doi.org/10.1016/j.gloplacha.2023.104336
Received 3 August 2023; Received in revised form 6 December 2023; Accepted 6 December 2023
Available online 12 December 2023

heatwaves over western Europe (Rousi et al., 2022), and the possible phenomenon of "Mediterranean Amplification" poses an additional threat (Brogli et al., 2021). Environmental and societal systems across much of the Mediterranean region are expected to reach tipping points by the end of this century (Cramer et al., 2018; Wunderling et al., 2023).

To contextualise recent and projected anthropogenic climate changes – and their ecological and societal consequences – proxy-based reconstructions need to span centuries to millennia robustly to capture the full range of high- to low-frequency natural climate variability (Essell et al., 2023). For this purpose, annually resolved and absolutely dated tree-ring chronologies represent the backbone of high-resolution paleoclimatology for much of the Northern Hemisphere extra-tropics (Büntgen et al., 2020, 2021; Esper et al., 2016; Ljungqvist et al., 2020).

Hitherto, millennial-long and well-replicated tree ring-based, warm-season temperature reconstructions have been derived from high-elevation or high-latitude sites at the cold distribution limit of upright tree growth (Esper et al., 2016). However, the climate signal in tree rings tend to fade towards lower latitudes (Büntgen et al., 2012; Galván et al., 2014; Touchan et al., 2017; Camarero et al., 2021), where hydroclimatic conditions are becoming the predominant control on xylogenesis (Ljungqvist et al., 2020). For the Mediterranean region, only the central Pyrenees and the highest mountains of the southern Balkans have so far yielded reliable temperature reconstructions from composite MXD chronologies (Büntgen et al., 2008, 2017; Esper et al., 2020). Further to their climatological relevance, and contrary to the strength of lower-resolution proxy archives (PAGES2k Consortium, 2019), tree-ring chronologies are most suitable to contribute to the interdisciplinary assessment of environmental and societal interrelationships at high spatiotemporal scales (Di Cosmo et al., 2017; Büntgen and Oppenheimer, 2020; Tegel et al., 2022). Such studies at the human-climate nexus that reach back to medieval times at annual resolution (McCormick et al., 2012), are, however, still missing for the Iberian Peninsula.

Here, we present an updated MXD chronology from the Spanish central Pyrenees, which not only prolongs previous versions back into medieval times and into the 21st century, but also consists of more samples in-between. To overcome the influence of decision-making in reconstructing climate (Büntgen et al., 2021), we apply a novel ensemble approach to refine our understanding of the course of past summer temperatures. Emphasis is placed on the investigation of the physical causes and societal consequences of summer temperature changes over the western Mediterranean region since medieval times. We therefore confront our new paleoclimate evidence against the forcing record from large volcanic eruptions, as well as newly compiled historical sources of military conflicts and wheat price changes.

Fig. 1. Sampling site. The Pyrenees Mountain range between France in the north and Spain in the south, with the "Lake Gerber" sampling site (red square) approximately 300 km east of the Atlantic Ocean and 200 km west of the Mediterranean Sea. Lake Gerber is located at 2166 m asl in the north-eastern part of the "Aigüestortes i Estany de Sant Maurici" National Park near Port de la Bonaigua (42°39′N and 00°58′E). The white dashed square refers to the 42–43°N and 0–2°E region for which gridded climate data were averaged, whereas the yellow star indicates the location of the Pic du Midi observatory (42°56′N, 0°08′E and 2830 m asl). Images at the bottom show different types of dry-dead, subfossil pine (*Pinus uncinata*) wood sampled between 2200 and 2400 m asl in steep, rocky terrain during our 2017 fieldwork. (For interpretation of the references to colour in this figure legend, the reader is referred to the web version of this article.)

2. Data and methods

The first continuous MXD-based summer temperature reconstruction from the Spanish central Pyrenees covered the period 1260–2005 CE (Büntgen et al., 2008). This dataset was composed of intra- and inter-annual MXD measurement series from 261 living and relict mountain pines (*Pinus uncinata* Ram.), which were collected in undisturbed upper treeline ecotones surrounding Lake Gerber (42°39′N and 00°58′E) in the north-eastern part of the "Aigüestortes i Estany de Sant Maurici" National Park near Port de la Bonaigua in the Spanish central Pyrenees (Fig. 1). Almost ten years later in 2017 CE, an update of this record not only increased the total number of MXD series to 414 (Büntgen et al., 2017), but also extended the temperature reconstruction to backwards to 1186 and forwards to 2014 CE. However, the early portion of the 2017 dataset was still tenuously replicated up to the mid-14th century, and the recent end date of the record in 2014 coincided with a putative hiatus in global warming (Medhaug et al., 2017). To further extend the Pyrenees MXD chronology back into medieval times and the 21st century, and to increase its sample size in-between, we conducted additional fieldwork in 2017 and 2021 at Lake Gerber (Fig. 1). Our sampling sites are located approximately 300 km east of the Atlantic Ocean and 200 km west of the Mediterranean Sea, close to the boarder with Andorra in the east and close to the boarder with France in the north. All samples come from steep, rocky terrain between 2200 and 2400 m asl, where relict pine wood can persist for centuries (Büntgen et al., 2008, 2017).

The updated MXD dataset we present here, consists of core and disc samples from 534 trees (Fig. 2), with individual start (end) years ranging between 924 (1353) and 2017 (2020) CE. Pith-offset estimates, based on a simple concentric circle model, are available for each sample. The mean series length of all 534 samples is 204 years, with minimum and maximum values of 4 and 732 years, respectively. The average MXD per measurement series is 0.64 g/cm^3 (Fig. 2), with minimum and maximum values of 0.44 and 0.84 g/cm^3, respectively. Each year between 1119 and 2020 CE is replicated by 6–240 MXD series (Fig. S1), with a mean of 99 samples per year. A mean series length of circa 300 years persists from the mid-13th to the mid-18th century (Fig. S1), whereas overall longer and shorter samples are found during the first and last 100 years of the chronology, respectively. MXD series were measured with high-precision Walesch 2003 X-ray densitometers at the Swiss Federal Research Institute (WSL) in Birmensdorf, Switzerland (Schweingruber et al., 1978; Eschbach et al., 1995), and at Johannes Gutenberg University (JGU) in Mainz, Germany (Esper et al., 2020). Wood density was determined in grams per cubic centimetre (g/cm^3), with sufficient resolution to work with slow growing conifers that may only produce a few tracheid cells in a single growing season. To avoid potential biases from stem-internal changes in fibre direction, each sample was cut into 2–4 cm long, and 1.23 mm thin sections perpendicular to the tracheids' longitudinal axis. The ratio between tracheid cell wall thickness and transverse cell lumen area, herein referred to as wood density, was continuously recorded within and between rings for each sample at a resolution of 0.01 mm (Björklund et al., 2019), and variations in X-ray image brightness were subsequently converted into g/cm^3.

Rather than selecting a single method for series detrending and chronology development (Fritts, 1976; Cook et al., 1995, 2005), we followed an integrative ensemble approach to evaluate and remove non-climatic, age-related trends in the raw MXD measurements and generate a suite of dimensionless timeseries. The ensemble approach further

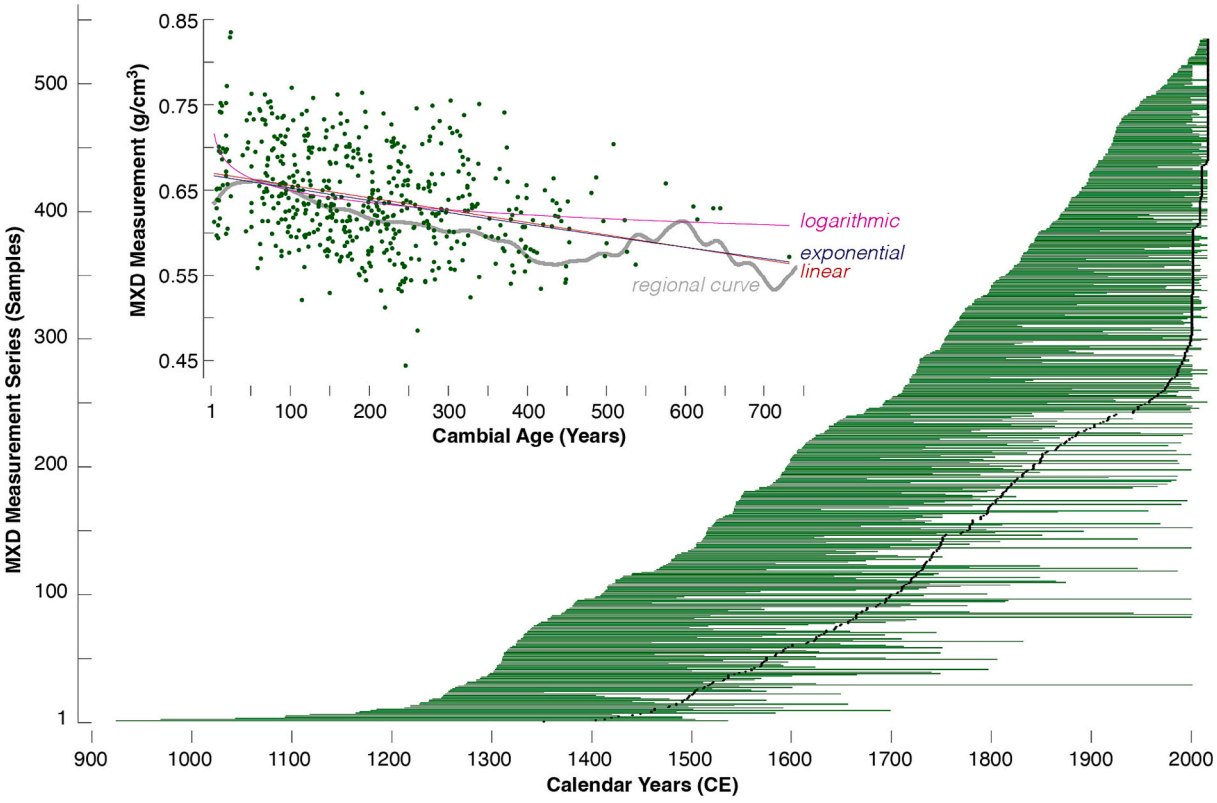

Fig. 2. Sample distribution. Temporal distribution of 534 maximum latewood density (MXD) measurement series sorted by their first ring (green horizontal bars), whereas the black dots show sample distribution when sorted by end dates. Series start dates range from 924 to 2017 CE, whereas the corresponding end dates are between 1353 and 2020 CE. The mean series length is 204 years, with minimum and maximum values of 4 and 732, respectively. The average MXD per series is 0.64 g/cm^3, with minimum and maximum values of 0.44 and 0.84 g/cm^3, respectively. Inset shows relationship between mean series MXD (g/cm^3) and total series length (years), which can be described as logarithmic ($R^2 = 0.0984$), exponential ($R^2 = 0.1002$), or linear ($R^2 = 0.1001$) functions. The grey curve is the regional curve (RC) after 50-year smoothing. (For interpretation of the references to colour in this figure legend, the reader is referred to the web version of this article.)

helped us to overcome the influence of decision-making (Büntgen et al., 2021), and we applied various versions of the Regional Curve Standardisation technique (RCS; Briffa et al., 1992; Esper et al., 2003), as well as single series detrending using cubic smoothing splines with 50% frequency cut-off at 200 years and 2/3 of the individual series lengths (Cook and Peters, 1981). Combined with index calculation as ratios or residuals after power transformation (Cook and Peters, 1997), these detrending options resulted in an ensemble of 32 slightly different MXD chronologies (Table S1). We then reduced the MXD dataset from 534 series to 494 series by removing all series that either contained less than 35 measurements, exhibited a negative first-order autocorrelation, had a mean MXD value below 0.5 or above 0.8 g/cm^3, or a combination thereof. The full ($n = 534$) and trimmed ($n = 494$) MXD datasets are very similar (Table S2), and only diverge marginally in their extreme minimum and maximum values. Following the same ensemble approach as described above, we created another suite of 32 MXD chronologies from the trimmed dataset. The minimum, mean, median and maximum MXD values from all 64 ensemble members were calculated for each year between 1119 and 2020 CE when sample size was at least six series. While the mean and median chronologies are almost identical ($r = 0.99$), the minimum and maximum chronologies exhibit level offset that is most pronounced before 1150 and after 2000 CE (Fig. S2A). The annual values of all timeseries, except for the maximum MXD chronology, are slightly skewed towards lower indices (Fig. S2B). The Expressed Population Signal (EPS; Wigley et al., 1984), hereinafter calculated over 31-year windows lagged by 15 years for the raw and detrended MXD measurement series, is on average 0.93 back to 1119 CE. EPS values fluctuate between 0.65 and 0.81 from 1170 to 1230, but range above 0.85 from the mid-13th century onwards.

Since all chronology versions contain variance changes over time (Fig. S2A), we further stabilized the year-to-year variability by dividing each annual value of the MXD records by its corresponding, centred 31-year standard deviation (Osborn et al., 1997; Frank et al., 2007a). The inner and outermost 15 years of the chronologies were stabilized using the average standard deviation of the following and previous 15 years of the timeseries. The final, variance stabilized ensemble (VSE) chronologies reflect stable high-frequency variability between 1119 and 2020 CE (Fig. S3A). Offset between the minimum and maximum VSE chronologies is largest before around 1320 and after 2000 CE (Fig. S3B). Although the different chronology versions with and without detrending and with and without additional variance stabilisation exhibit similar trends and extremes over the past nine centuries (Fig. S4), we consider the median (rather than the almost identical mean) VSE MXD chronology to be the ideal reflection of past summer temperature variation on interannual to multi-centennial timescales (though performed the proxy-target comparison with both indices).

For signal detection and climate reconstruction, we investigated four gridded land surface temperature products averaged over 42–43°N and 0–2°E (Fig. 1). These data cover the central Pyrenees with our study site being right at their centre. The highest spatial resolution of 0.25° is provided by *E*-OBS (v25.0e) spanning 1920–2022 (Cornes et al., 2018). The CRU (TS4.06) and CRUTEM (5.0) afford a spatial resolution of 0.5° and 5.0° for 1901–2021 and 1850–2022 (Harris et al., 2020), respectively. The Berkeley interpolation is available at 1.0° spatial resolution and extends back to 1750 CE (Rohde and Hausfather, 2020). For each of these products, their monthly mean temperatures, within the area defined above, were transformed into anomalies with respect to 1961–90 CE. Ten seasonal temperature means of at least two consecutive monthly mean values between May and September were computed: May–June (MJ), May–July (MJJ), May–August (MJJA), May–September (MJJAS), June–July (JJ), June–August (JJA), June–September (JJAS), July–August (JA), July–September (JAS), and August–September (AS). The MJJAS mean and median temperatures from the CRU, CRUTEM and Berkeley products are almost identical (Fig. S5), but the *E*-OBS anomalies are around 1.0 °C warmer before 1950 CE and around 0.5 °C cooler after the mid-1990s when compared to all other records. This offset becomes even more evident when considering moving correlations between the different datasets and comparing linear trends of the timeseries (Fig. S6).

In addition to the freely available and highly recognised gridded products, we obtained daily temperature measurements from the nearby summit observatory at Pic du Midi in the French Pyrenees (Dessens and Bücher, 1995) (Fig. 1). Located at 42°56' North, 0°08′ East and 2830 m asl, the unique high-elevation station started recording daily minimum and maximum temperatures as early as October 1881 CE, while daily mean temperatures are only available since January 1949. Daily minimum and maximum temperatures were used to estimate daily mean temperatures when those were not recorded, i.e., (Tmin + Tmax) / 2 (Štěpánek et al., 2011). Surrounding high-elevation stations above 1000 m asl and within a search radius of 1200 km were used for gap filling (Klein Tank et al., 2002), quality control, and data homogenization (Štěpánek et al., 2013). Despite a rather marked increase in warm season temperatures from 1985 to 86 CE that coincides with a major shift in the North Atlantic Oscillation (NAO; Büntgen et al., 2022a), no significant breakpoint was detected in the monthly mean Pic du Midi temperature timeseries over the past 142 years (Fig. S7A). We further applied a mean summer lapse rate of 0.5 K per 100 m altitudinal difference (Büntgen et al., 2022b) to approximate absolute monthly and seasonal temperature means representative for our sampling site at Lake Gerber (Fig. S7B).

The mean and median VSE MXD chronologies were correlated against monthly and seasonal temperature anomalies, and we used a moving-window approach to assess stability in the observed proxy-target relationship over time. We then scaled the median VSE MXD chronology against the corresponding median of the four MJJAS temperature means over 1920–2020 CE, for which all four gridded products have data and their median could be calculated. The mean and variance of the MXD proxy data were therefore adjusted to the mean and variance of the meteorological target data. This simple calibration technique is less susceptible to variance underestimation than direct regression (Esper et al., 2005), and less prone to variance overestimation by indirect regression. Error bars associated with our new reconstruction integrate series detrending and chronology development uncertainty obtained from the ensemble approach (Büntgen et al., 2021), uncertainty due to changing sample size over time, the amount of unexplained variance in the calibration period expressed by the Root Mean-Square Error (RMSE), as well as the uncertainty obtained from the four different gridded MJJAS target products. For calibration-verification trials, we calculated the Coefficient of Efficiency (CoEf) and Reduction of Error (ReEr) statistics over the full and two early/late split periods (Cook et al., 1999). ReEr determines if the proxy-based temperature estimates are better than the instrumental temperature mean in the calibration period, while CoEf is an even more rigorous criterion referring to the instrumental mean of the verification period. Ranging from 1 to -∞, positive ReEr and CoEf values indicate reconstruction skill. We also calculated the Durbin-Watson (DW; Durbin and Watson, 1951) statistic to assess autocorrelation in the proxy-target timeseries' residuals, with DW values close to 2 denoting a stable relation.

Superposed Epoch Analysis (SEA; Chree, 1913) was applied to quantify the interannual behaviour of the reconstructed summer temperature anomalies in relation to 20 large volcanic eruptions (Table S3). Out of these events (Büntgen et al., 2017), 11 have known and nine estimated dates, and source volcanoes are either identified (7), putative (5), or unknown (8). This set of the assumed largest tropical or Northern Hemisphere extra-tropical eruptions is based on the approximate coincidence of peaks in volcanic forcing timeseries (Sigl et al., 2015). Temporal mismatch of up to three years during the time of interest can be accommodated by persisting dating uncertainties in the ice core sulphur record and temporal offsets between eruption timing, peak radiative forcing, surface temperature anomalies, and volcanic aerosol deposition in the polar regions (Esper et al., 2013; Torbenson et al., 2015). Split-period SEA of the reconstructed summer temperature

anomalies was applied for 15/5 pre-industrial/industrial eruptions </>1750 CE. Bootstrap spectral analysis was used to detect possible cyclic behaviour in our reconstruction (Percival and Walden, 1993) via the "tseries" R package (Trapletti et al., 2023). We further compared our new reconstruction against the two previous MXD-based studies from Lake Gerber (Büntgen et al., 2008, 2017), as well as a comparable MXD record from Mount Smolikas in northern Greece (Esper et al., 2020). A regional subset of the "Old World Drought Atlas" (OWDA; Cook et al., 2015), centred over Lake Gerber was selected for hydroclimatic comparison between 42.25° North and 0.75° East.

As an exploration of possible relationships between climate and conflict, we compared our reconstruction against a newly compiled record of military conflicts and engagements in Iberia going back to the early 12th century (Lomax, 1978; Reilly, 1993; Glete, 2001; O'Callaghan, 2003; Kamen, 2005; O'Callaghan, 2014; Catlos, 2018; García Fitz and Gouveia Monteiro, 2018). Although armed conflicts varied in their scale and impact, we represent them in a simple binary manner, with '1' signifying at least one military conflict per year and '0' standing for a lack of such. The combined series was converted into visualised clusters of frequent conflicts and 'peaceful' periods. Drawing primarily on published records from historical archives in Barcelona that cover the period from 1283 to 2000 CE (Feliu, 1991; Argilés i Aluja, 1999; Jacks, 2006; Carreras and Tafunell, 2005; Franklin-Lyons, 2009; Maltas i Montoro, 2019), we developed a long-term record of annual wheat price changes in Catalonia, northeast Spain. To investigate possible temperature effects, we represented each year's price as a 12-month average of the Catalan agricultural year running from the start of the harvest period in June of the previous year to its end in May of the current year. We further expressed each price value as a relative percentage of the preceding 5-year average. As previously reported in studies of historical food crises and famines (Slavin, 2016; Benito i Monclús, 2016; Slavin, 2019; Franklin-Lyons, 2022), we recognise that crop prices tend to rise more because of indirect societal and institutional factors, including hoarding, speculation, market failure and conflict, rather than as a direct result of failed harvest. Nevertheless, we also acknowledge that climate factors can act as initial triggers of grain price variations (Esper et al., 2017a; Ljungqvist et al., 2023), with anthropogenic factors usually intensifying subsequent food crises. Hence, disentangling environmental triggers from societal factors in this regard remains challenging, and caution is advised for any interpretation.

3. Results

The mean and median VSE MXD chronologies correlate significantly positively at the 99.9% confidence limit with monthly mean temperatures of May, June, and August between 1920 and 2020 CE (Fig. S8A). Slightly lower correlations are found with April, July, and September temperatures, whereas monthly means before and after the growing season are non-significant. Similar patterns are exhibited by the mean and median VSE MXD chronologies, as well as by the four gridded products. Correlation coefficients between the VSE MXD chronologies and the monthly May, June, and August temperature means slightly increase when using the 1950–2020 CE period, for which the meteorological observations are most reliable (Fig. S8B). While non-significant proxy-target correlations between October and March suggest that temperature changes outside the growing season are irrelevant, low correlations with July conditions most likely imply that peak summer temperatures are always warm enough so that year-to-year changes do not affect the latewood formation at our site. The observed low correlations with July temperatures, however, do not necessarily mean that summer warmth is not relevant for the development of MXD.

Correlation coefficients between the MXD chronologies and ten seasonal temperature averages of at least two consecutive monthly mean values between May and September reveal the highest proxy-target association for the complete May–September (MJJAS) growing season (Fig. S9A). Using the mean and median VSE MXD chronologies, four gridded products and two calculation periods back to 1920 and 1950 CE, correlations with MJJAS vary from 0.71–0.77, with the highest association found between the median VSE MXD chronology and the *E*-OBS data spanning 1950–2020 CE (Fig. S9B). The lowest correlations are exhibited by the short windows of June–July and July–August, during which high-summer temperatures at the upper treeline in the Spanish central Pyrenees are likely too warm to affect the xylogenesis of *Pinus uncinata* at Lake Gerber negatively. In fact, the estimated absolute July mean temperatures are exceeding 9 and 10 °C since 1930 and 1990, respectively (Fig. S7B). Moving 31-year correlation coefficients between the median VSE MXD chronology and the four gridded MJJAS temperature records reveal temporal stability in the proxy-target relationship over the past 100 years (Fig. S10A), during which correlations range between around 0.6 and 0.8. Moving 31-year correlations exceeding 0.8 are found with *E*-OBS in the 1950s and 1960s. The proxy-target dependency during the 20th and early-21st century appears even more stable when extending the moving correlations back to 1750 CE (Fig. S10B), for which only Berkeley data are available. This visual and statistical long-term comparison indicates a dramatic decrease in the quality of the gridded product before around 1800 CE, when meteorological information for the western Mediterranean region must be interpolated from a few stations located in central Europe and northern Italy.

There is remarkable proxy-target agreement on interannual to multidecadal timescales after scaling the median VSE MXD chronology against the median of the four gridded MJJAS temperature means over the common period 1920–2020 CE (Fig. 3A). Significant ($p < 0.001$) correlation coefficients are 0.67 and 0.76 for two independent split periods before and after 1970 CE. The proxy-target association increases to $r = 0.83$ after 20-year low-pass filtering (1920–2020 CE), which is partially related to the high autocorrelation of smoothed data. The reconstructed and measured summer temperatures are rather stable from around 1920–1950, followed by a decline in the anomalously cool 1970s, after which temperatures rise again from 1972 to 2003 CE. Relatively stable summer temperatures are characteristic for the early-21st century until at least 2020 CE. All calibration-verification trials reveal high reconstruction skills (Table S4), with ReEr and CoEf values ranging from 0.31–0.57, and DW statistics between 1.81 and 1.91. Although MJJAS temperatures from the Pic du Midi observatory confirm the course of the gridded and reconstructed data, the high-elevation station measurements are circa 0.5 °C warmer between 1985 and the 1990s. Spatial correlation maps of the MXD proxy against gridded land surface MJJAS temperatures from *E*-OBS describe significant ($p < 0.001$) agreement over western-central Europe and the Mediterranean basin back to 1950 CE (Fig. 3B). Correlation coefficients >0.6 are found over Spain, southern France, Italy, parts of the Balkans, and north-western Africa. A similar geographic pattern is obtained when replacing the MXD proxy with MJJAS temperature measurements from the Pic du Midi station (Fig. 3C). By no surprise, the spatial domain of explained summer temperature variability increases substantially over north-west Africa, as well as into the Near East and the Arabian Peninsula when using CRU instead of *E*-OBS data (Fig. S11). Further to the explained land surface temperature variability, the MXD proxy reveals significant ($p < 0.001$) positive correlations with MJJAS sea surface temperatures in the Mediterranean Sea and the nearby Atlantic Ocean from the Canary Islands in the south to the Bay of Biscay in the north (Fig. S12).

Continuously spanning from 1119 to 2020 CE and representing the western Mediterranean region, our new reconstruction – based on simple scaling of the median VSE MXD chronology against the median of MJJAS temperature anomalies averaged over four gridded products from 1920 to 2020 CE – exhibits a slight long-term warming trend ($p < 0.01$) that culminates in unprecedented warmth since 2003 CE (Fig. 4). The reconstruction has a low first-order autocorrelation of 0.08, and uncertainty ranges fluctuate around 2.0 °C between 1320 and 2000 CE, but almost double before and after. Uncertainty of our reconstruction is below 1.5 °C from around 1350–1370, 1450–1590, and again from 1790

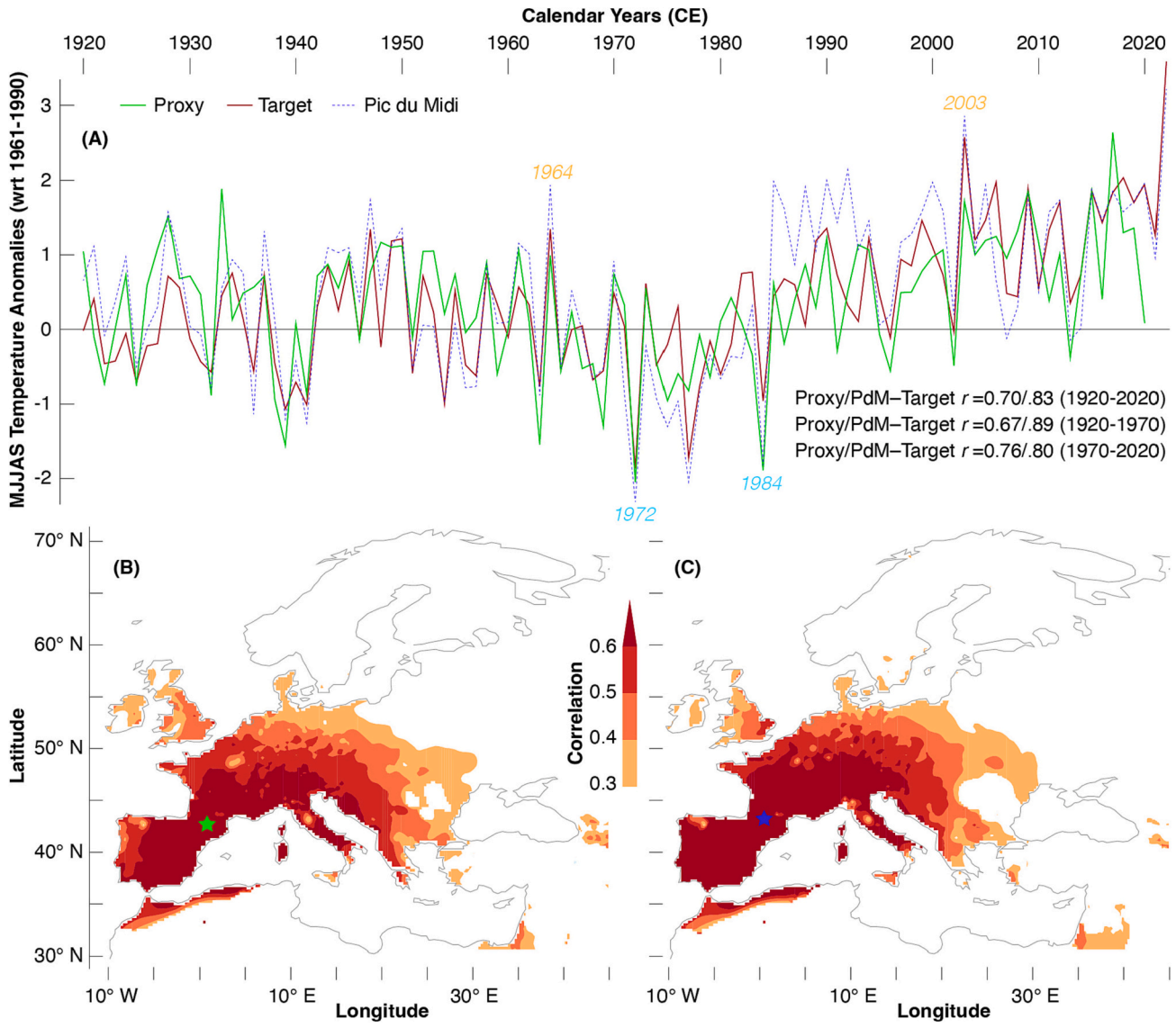

Fig. 3. Proxy-target agreement. (A) Comparison of the proxy-based reconstructed (green) and grid-based measured May–September (MJJAS) temperatures expressed as anomalies with respect to the 1961–90 CE mean, together with MJJAS measurements from the Pic du Midi (PdM) high-elevation station (see Fig. 1 for details). Correlation coefficients between the proxy (and PdM) and target data over the full and two earl/late split periods are provided at the lower right (see Table S4 for calibration-verification statistics). (B) Spatial correlation coefficients between our new reconstruction (green star) and gridded (0.25° lat/lon) land surface MJJAS temperatures (1950–2020 CE) from *E*-OBS. (C) Similar to (B) but using MJJAS temperatures from the Pic du Midi station (blue star). (For interpretation of the references to colour in this figure legend, the reader is referred to the web version of this article.)

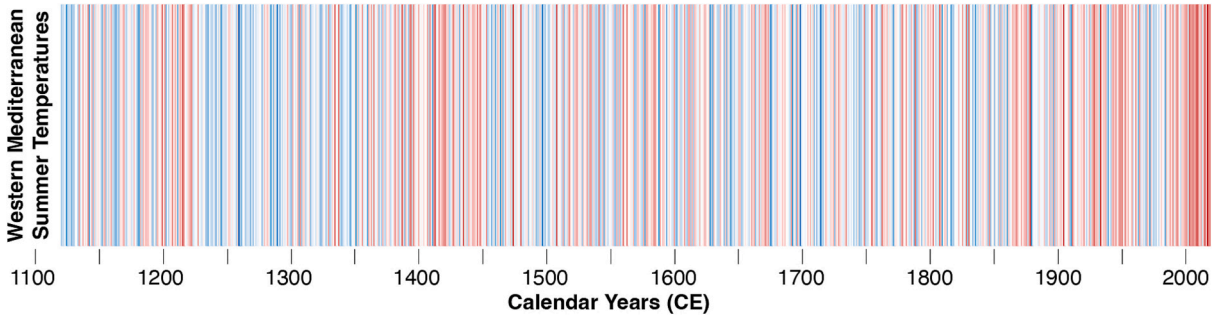

Fig. 4. Western Mediterranean summer temperature reconstruction. May–September (MJJAS) temperature anomalies reconstructed for 1119–2020 CE and expressed as colour stripes from cold to warm (blue to red). (For interpretation of the references to colour in this figure legend, the reader is referred to the web version of this article.)

to 1870 CE.

Clusters of relatively warm pre-industrial summers are evident around 1200, between the 1380s and 1560 (Fig. 5A), as well as around 1760 CE, whereas extreme cold summers are more evenly distributed over time. Our new reconstruction reveals four warm periods before the 1220s, between the 1380s and 1430s, from the 1870s to the 1940s, and again since around 2000 CE. Five phases of anomalously cold summers are found between the 1240s and 1280s, in the 1340s, the 1490s, around 1700 and again in the 1970s CE. The warmest reconstructed MJJAS temperature anomaly relative to 1961–90 is found in 2017 (2.6 ± 2.2 °C), and the warmest pre-industrial summer is 1473 (2.0 ± 1.1 °C). Four of the 20 warmest summers occur between 2003 and 2017 CE (see Table 1 for the extremes), but the measured MJJAS temperature anomaly in 2022 (3.6 ± 0.3 °C) clearly exceeds all the reconstructed summers. The coldest reconstructed MJJAS temperature anomaly is found in 1258 (−3.4 ± 1.4 °C), followed by 1714 (−2.8 ± 1.1 °C), and 1288 (−2.8 ± 1.5 °C). The largest interannual increase in MJJAS temperatures occurs from 1910 to 11 (3.3 ± 0.1 °C), whereas the largest drop from one summer to the next is found from 1257 to 58 (−4.0 ± 0.1 °C).

A closer look at year-to-year anomalies emphasises stability of the reconstructed high-frequency variance over time (Fig. S13A). The two warmest and coldest consecutive summers are 2017/18 (2.0 ± 2.2 °C) and 1258/59 (−2.2 ± 1.3 °C), respectively. The two-year consecutive amplitude in the reconstructed MJJAS temperature anomalies reinforces the long-term warming trend of the final reconstruction with marked multi-decadal variability superimposed (Fig. S13B). The five warmest decadal blocks are found at the recent end of the reconstruction with

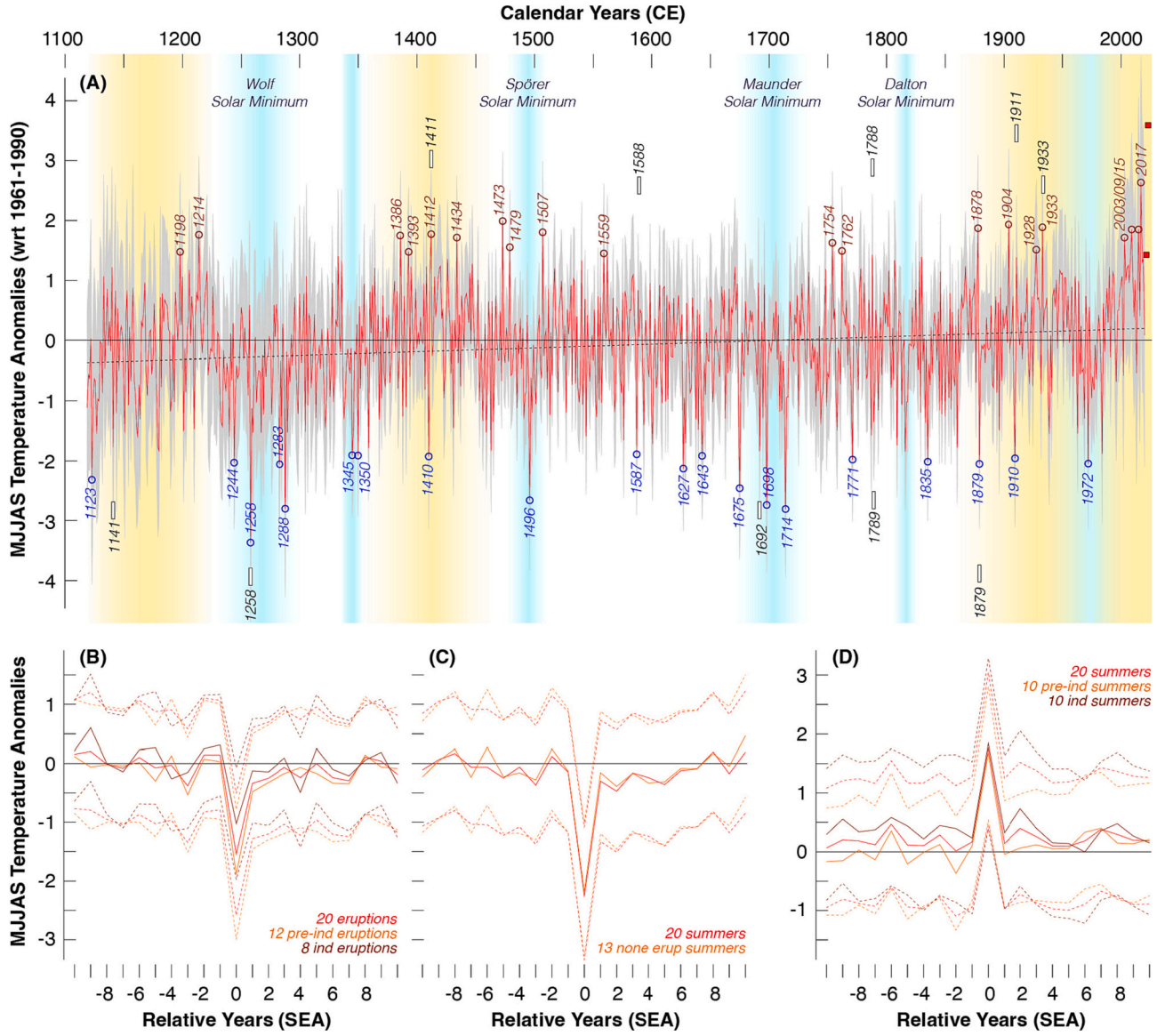

Fig. 5. Reconstructed summer temperature variability. (A) May–September (MJJAS) temperature anomalies reconstructed for 1119–2020 CE, with generally warmer and cooler periods emphasised by orange and blue shadings. Red squares at the right are the 2021/22 instrumental MJJAS temperature measurements. Dashed grey line shows long-term warming. The 20 warmest and coldest summers (red and blue circles), as well as the ten most extreme year-to-year temperature fluctuations (black rectangles) are indicated (Table 1). (B) Average response of our reconstruction to large volcanic eruptions (Table S3), and after splitting into pre-industrial and industrial eruptions </> 1760 CE (dotted lines), with the relative SEA year 0 referring to peak cooling after the eruption, e.g., 1816 in case of the Tambora eruption in April 1815 and 1258 in case of the Samalas eruption in 1257. (C) Average behaviour of our reconstruction during the coldest summers, and after excluding those years that were following volcanic eruptions (dotted lines). (D) Average behaviour of our reconstruction during the 20 warmest summers, and after splitting into ten pre-industrial and industrial summers (dotted lines). (For interpretation of the references to colour in this figure legend, the reader is referred to the web version of this article.)

Table 1
Reconstructed temperature extremes.

(A)			(B)		
	Warmest Summer	Coldest Summer		Warmest Summer Chan	Coldest Summer Chan
	2017 (2.6 +/− 2.2)	1258 (−3.4 +/− 1.4)		1910–11 (3.3 +/− 0.1)	1257–58 (−4.0 +/− 0.1)
	1473 (2.0 +/− 1.1)	1714 (−2.8 +/− 1.1)		1410–11 (3.0 +/− 0.2)	1878–78 (−3.9 +/− 0.1)
	1904 (1.9 ±1.3)	1288 (−2.8 +/− 1.5)		1787–88 (3.0 +/− 0.1)	1140–41 (−3.0 +/− 0.1)
	1933 (1.9 ±1.3)	1698 (−2.7 +/− 1.1)		1932–33 (2.8 +/− 0.2)	1691–92 (−2.8 +/− 0.1)
	1878 (1.9 ±1.2)	1496 (−2.7 +/− 1.2)		1587–88 (2.7 +/− 0.1)	1788–89 (−2.8 +/− 0.1)
	2015 (1.9 ±2.2)	1675 (−2.5 +/− 1.2)	(C)		
	2009 (1.8 ±1.6)	1123 (−2.3 +/− 1.8)		Warmest Con Summers	Coldest Con Summers
	1507 (1.8 ±1.2)	1627 (−2.1 +/− 1.0)		2017–18 (2.0 +/− 2.2)	1258–59 (−2.2 +/− 1.3)
	1412 (1.8 ±1.1)	1283 (−2.1 +/− 1.3)		2008–09 (1.6 +/− 1.6)	1714–15 (−1.9 +/− 1.0)
	1214 (1.8 ±1.3)	1879 (−2.1 +/− 1.1)		2016–17 (1.5 +/− 2.2)	1179–80 (−1.8 +/− 1.4)
	1386 (1.7 ±1.1)	1972 (−2.0 +/− 1.1)		2009–10 (1.5 +/− 1.6)	1713–14 (−1.8 +/− 1.0)
	2003 (1.7 ±1.3)	1244 (−2.0 +/− 1.1)		1877–78 (1.4 (+/− 1.1)	1287–88 (−1.8 +/− 1.3)
	1434 (1.7 ±1.0)	1835 (−2.0 +/− 1.0)	(D)		
	1754 (1.6 ±1.2)	1771 (−2.0 +/− 1.0)		Warmest Sum Decade	Coldest Sum Decade
	1479 (1.6 ±1.0)	1910 (−2.0 +/− 1.2)		2003–12 (1.2 +/− 1.5)	1120–29 (−1.0 +/− 1.7)
	1928 (1.5 ±1.2)	1410 (−1.9 +/− 1.2)		2001–10 (1.1 +/− 1.5)	1119–28 (−1.0 +/− 1.7)
	1762 (1.5 ±1.1)	1643 (−1.9 +/− 1.1)		2008–17 (1.1 +/− 1.8)	1282–91 (−1.0 +/− 1.3)
	1393 (1.5 ±1.1)	1350 (−1.9 +/− 1.0)		2009–18 (1.1 +/− 1.9)	1283–92 (−1.0 +/− 1.3)
	1198 (1.5 ±1.3)	1345 (−1.9 +/− 1.0)		2000–09 (1.1 +/− 1.4)	1158–67 (−1.1 +/− 1.4)
	1559 (1.5 ±1.2)	1587 (−1.9 +/− 1.0)			

(A) The 20 warmest and coldest reconstructed May–September (MJJAS) temperature anomalies between 1119 and 2020 CE (with respect to 1961–90 CE). (B) The five largest positive (warm) and negative (cold) summer-to-summer temperature changes, (C) the five warmest and coldest consecutive summers, and (D) the five warmest and coldest decades.

start dates between 2000 and 2009 CE (Table 1). Three of the five coldest decadal blocks occur at the beginning of the record with start dates between 1119 and 1158 CE.

Focusing on each century separately, the 12th century is characterised by a general warming trend (Fig. 5A). The coldest summers are 1123, 1141 and 1179/80 CE, and the warmest summer of the 12th century is 1198 CE. The early 13th century exhibits a sequence of very warmer summers until the 1220, followed by a cooling trend over three decades. Abrupt cold spells occur in 1210, 1258 and 1288, and the warmest summer of the 13th century is 1214 CE. The first half of the 14th century is relatively cool and stable, whereas more interannual variability is found afterwards. Distinct coldest summers are 1345, 1350 and 1359 CE, and the warmest summer of the 14th century is 1386 CE. The first half of the 15th century is relatively warm and stable, whereas cooler conditions and more year-to-year variability start in the 1450s, with the temperatures dropping again from the 1480s onwards. Distinct cold spells occur in 1410 and 1431, and there is a marked cluster of cold summers in 1456, 1459 and 1463. The warmest and coldest summers of the 15th century are 1473 and 1496 CE. The 16th century is unusually stable without any long-term trend. Though inconsiderable, the warmest and coldest summers of the 'flat' 16th century are 1507 and 1587 CE. The 17th century is characterised by a modest long-term warming trend until 1673, followed by a sharp temperature depression and cooling until the end of the century. Marked cold spells occur in 1627 and 1675 and 1698, with the latter being the coldest summer. Though not distinct, 1671 is the warmest summer of the 17th century. The 18th century exhibits a remarkable cooling trend starting around 1704 and culminating in 1714, which also marks the coldest summer of the century. More abrupt cold spells occur in 1725, 1744, 1758, and 1771. The warmest summer of the unstable 18th century is 1754 CE. While not displaying any long-term trend, the 19th century is characterised by distinct summer cooling in 1809 and 1816, as well as 1835, 1860 and 1879. Since the warmest summer of the 19th century is 1878, there is an exceptional year-to-year drop in mean summer temperature of almost 4 °C from 1878 to 1879 CE. The 20th century is relatively stable until around 1960. Overall colder summers cluster between 1965 and 1984, after which the recent warming peaks in the warmest reconstructed summer in 2017 CE. The coldest summers of the 20th century are in 1910, 1972 and 1984, whereas the warmest summers of the first half of the 20th century are 1904 and 1933 CE.

After the coldest reconstructed summer that followed the Samalas eruption in 1257 CE (part of Rinjani volcano in Indonesia), the MJJAS temperatures take approximately 20 years to 'recover' from the rapid drop to −3.4 °C in 1258 CE (Fig. 5A). There is an average cooling of −1.5 (±1.0) °C following 20 large volcanic eruptions since medieval times (Fig. 5B). When splitting the event years in 12 and eight eruptions before and after 1760 CE (Table S3), the average pre-industrial/industrial cooling is −1.9/−1.0 (±1.1/0.9) °C. Independent of their forcing, the 20 coldest reconstructed summer temperature anomalies average − 2.3 (±1.3) °C (Fig. 5C), and a similar cooling of −2.2 (±1.2) °C is exhibited by the 13 coldest summers for which no volcanic eruptions have been reported. Although there is a rapid recovery after the coldest summers, temperatures remain slightly below average for about eight years. By contrast, the 20 warmest reconstructed summers average 1.8 (±1.3) °C (Fig. 5D), and there is no obvious difference after segmenting pre-industrial and industrial periods, and there is no positive lag effect on the following years.

Comparisons of our new reconstruction with two previous summer temperature records from the same region that share a substantial amount of data (B08 and B17; Büntgen et al., 2008, 2017) reveals strong agreement (Fig. 6A). Significant positive correlation coefficients of 0.93 and 0.97 with B08 and B17 over the common period 1260–2005 CE are not surprising due to substantial data overlap between the three MXD-based reconstructions. Correlations slightly decrease to 0.86 and 0.89 (for B08 and B17) after 50-year low-pass filtering. The previous reconstructions reflect slightly more amplitude on multi-decadal timescales, with the largest differences between around 1350 and 1450 CE, which could be a result of inappropriate variance stabilisation during periods of low sample size in B17 and especially in B08. Intriguingly, we find strong mid-frequency coherency between our MJJAS temperature reconstructions from the central Pyrenees and a comparable, MXD-based study from the southern Balkans (Fig. S14). After 50-year low-pass filtering, both summer temperature reconstructions correlate at 0.52 over their common period 1119–2015 CE, share multi-decadal variability and exhibit a similar long-term warming trend since medieval times.

Comparison of our reconstruction with newly compiled historical evidence from the Iberian Peninsula suggests a lack of military conflict during or following both, exceptionally hot and exceptionally cold summers (Fig. 6A, Table S5). Overall, summer temperatures in those 224 years for which military conflict has been reported average − 0.21 °C compared to −0.02 °C in all other years between 1119 and 2020 CE (Fig. 6 inset). Taking the period 1119–1492 CE that represents the most intense phase of turmoil when at least 142 out of 374 years saw interfaith or internecine conflicts, no military engagements are reported in the six years with the hottest summers (>1.5C°), and only one out of twelve years with mean MJJAS temperature anomalies >1.25C° (1333)

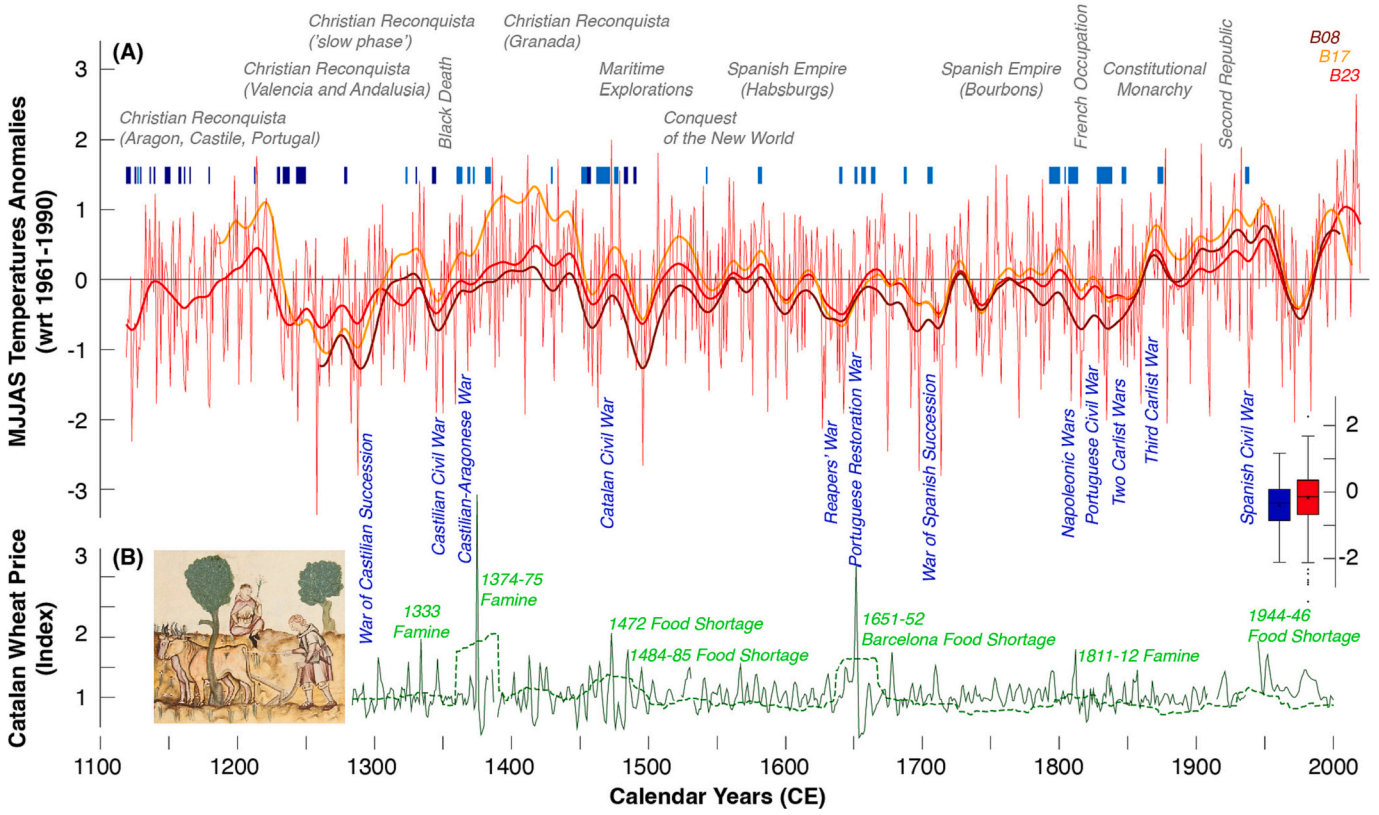

Fig. 6. Temperature variability and human history. (A) Comparison of our new temperature reconstruction (B23) against two previous summer temperature records from the central Spanish Pyrenees (B08, B17; Büntgen et al., 2008, 2017) after smoothing with 50-year low-pass filters (thick lines). Major historical events relevant to Iberia are listed in grey, whereas the largest and most important armed conflicts are indicated in blue. The blue vertical stripes show the timing of reported military conflicts on the Iberian Peninsula that took place between Christians and Muslims (dark blue) and amongst Christians (light blue) (all data are provided in Table S5). The inset boxplots on the right show temperature differences between years with and without military conflict (blue and red). (B) Annual wheat price changes in Catalonia relative to the previous 5-year average (dark green line), together with its 31-year moving standard deviation (dashed line). Major famines and food shortages on the Iberian Peninsula are indicated in light green, and inset depicts rural life in medieval Spain, taken from the 'Cantigas de Santa María' written during the reign of Alfonso X (1221–84 CE). (For interpretation of the references to colour in this figure legend, the reader is referred to the web version of this article.)

saw fighting. Although cold years did not preclude military unrest at the same level, no conflicts are reported for or after the three years with the coldest summers during that period (1123, 1258 and 1288, with respective anomalies of −2.32, −3.37 and − 2.80C°). More generally, we recognise a tendency of less conflicts occurring during relatively warm periods from ~1190–1220, ~1390–1450, as well as in the 16th and 18th and 20th centuries (Table S5).

Moreover, we find that Catalan wheat prices are more stable when summer temperatures range above average (Fig. 6B). Extreme instances of wheat price changes, however, occur in 1333/34 that is known as 'lo mal any primer' (or the 'first bad year'), as well as in 1412/13, 1473/74, 1540/41, following anomalously hot summer temperatures, and 1345/46, 1463/64, 1629/30, 1643/44, 1809/10, and 1835/36, following rather cold summer temperatures. Except for 1412/13 and 1473/74, associated with unusually hot summers, these high price years follow either excessive dry or wet months (based on the OWDA; Cook et al., 2015), as it was in 1333/34 (dry), 1345/46 (wet), 1463/64 (wet), 1643/44 (wet), 1809/10 (wet) and 1835/36 (wet). Indeed, there are numerous instances, when high prices resulted from hydroclimatic extremes during which summer temperatures were near average, such as 1374/75 (wet), 1420/21 (dry), 1483/84 (dry), 1643/44 (wet), 1651/52 (wet), 1677/78 (wet), 1945/46 (dry), 1950/51 (dry), and 1952/53 (dry) CE.

4. Discussion and conclusions

The updated MXD chronology from the Spanish central Pyrenees comprises of 534 individual wood samples of slow-growing and well-preserved living and relict mountain pines from upper treeline ecotones. In addition to site selection and signal detection, much weight has been given to series standardisation, i.e., detrending, for tree ring-based climate reconstruction (Fritts, 1976; Esper et al., 2016). However, the importance of additional variance stabilisation of single tree-ring chronologies (Osborn et al., 1997), or larger networks of chronologies (Frank et al., 2007a), has received less attention. In this study, we show that high sample size and temporally well distributed start and end dates of the individual MXD series make the detrending choice less important. In fact, we found essentially no difference between the raw and detrended chronologies (Fig. S4). Caution is advised since little influence of different detrending techniques requires massive sample size and an even distribution of series start and end dates (Fig. 2), but certainly does not apply for most tree-ring datasets for which appropriate detrending remains essential.

To mitigate the effects of decision-making (Büntgen et al., 2021), and to refine our understanding of the full range of past interannual to multi-centennial summer temperature variability over the western Mediterranean region for which high-resolution paleoclimate data are sparse (Luterbacher et al., 2012; Touchan et al., 2017), we applied a novel ensemble reconstruction approach that generates a suite rather than a single chronology. The minimum and maximum values of the ensemble members for each year were considered for final error estimation. The median VSE MXD chronology correlates significantly with gridded MJJAS temperature means over the western Mediterranean region ($r = 0.76$; $p \leq 0.001$). While the proxy-target relationship is stable back to around 1880 CE (Fig. S10), decreasing correlation during the 19th and

particularly the 18th century almost certainly relates to the decreasing number of meteorological stations in the western Mediterranean region. There are only a few stations in central Europe and three sites in Italy that provide continuous recording since the second half of the 18th century (Jones and Moberg, 2003; Frank et al., 2007b), but no such data exist for the Iberian Peninsula and northern Africa. Documentary meteorological evidence from Cádiz in southern Spain is a rare exception (Barriendos et al., 2002). Another meteorological exception is the high-elevation summit observatory at Pic du Midi in the French Pyrenees (Fig. 1), which started recording in 1881 CE. Intriguingly, the Pic du Midi measurements from 2830 m asl are not included in large-scale gridded products and largely under researched.

Although proxy-target correlations increase to 0.80 when using average May–June and August–September temperature means, we consider the complete MJJAS window more meaningful physiologically (for understanding stem xylogenesis), ecologically (for explaining forest growth), meteorologically (for reconstructing summer temperature), and socioeconomically (for exploring the human-climate nexus). Non-significant proxy-target correlations with July temperatures do not preclude the relevance of peak summer warmth for MXD development in *Pinus uncinata* at the upper treeline in the Spanish central Pyrenees (Büntgen et al., 2017). On the contrary, the observed bi-seasonal pattern only shows that even small temperature fluctuations at the beginning and at the end of xylogenesis affect MXD values (Fig. S7B), whereas July conditions are always warm enough. This simple explanation is corroborated by an experiment at the Swiss treeline that revealed no effects of systematic cooling on cell formation and cell wall lignification during the warm summer months (Körner et al., 2023), though in the cooler transition zone at the beginning of the growing season (Büntgen, 2023). Strong enough cold spells during the growing season have been demonstrated to trigger so-called Blue Rings in *Pinus uncinata* from Lake Gerber (Piermattei et al., 2020), which often occur after large volcanic eruptions when growing season temperatures drop.

The coldest reconstructed summer in 1258 follows the Samalas eruption on Lombok Island, Indonesia (Lavigne et al., 2013), which likely occurred between May and July 1257 CE. This explosive eruption resulted in one of the largest perturbations of stratospheric aerosol in the past 2000 years and led to widespread summer cooling across the Northern Hemisphere mid-latitudes (Oppenheimer, 2003; Sigl et al., 2015; Büntgen et al., 2022c). The next two coldest reconstructed summers are in 1714 and 1288 CE (-2.8 ± 1.1 °C and -2.8 ± 1.5 °C, respectively), though neither of them appears associated with volcanism from inspection of the ice core-based reconstructions of stratospheric aerosol optical depth and radiative forcing (Sigl et al., 2022). An 'enigmatic' eruption is registered circa 1285/86 but a reddish lunar eclipse recorded on the 22nd of October 1287 CE in England and Italy (Guillet et al., 2023) somehow suggests that parts of the stratosphere were less perturbated so the cold summer of 1288 evident in our reconstruction is less likely related to volcanic forcing. The comparability of cold summers with and without volcanic forcing suggest that the post-eruptive signal does not differ greatly from anomalies reflecting internal variability, highlighting the significance of Superposed Epoch Analysis (SEA). The general response of our new reconstruction to large volcanic eruptions and the overall behaviour during the coldest and warmest extremes emphasises the rapid recovery on interannual timescales (Fig. 5B-D), which is a common feature of MXD-based temperature reconstructions (Büntgen et al., 2006; Esper et al., 2012; Schneider et al., 2015; Stoffel et al., 2015). The reduced biological memory of MXD may not only improve the dating precision of ice core-derived volcanic forcing records but possibly also help to detect yet unknown volcanic eruptions (Esper et al., 2017b; Schneider et al., 2017), which is important because we know the sources and dates of only a handful of pre-industrial volcanic eruptions (Table S3). The autocorrelation ($r = 0.08$) of our reconstruction suggests that we are not overestimating low-frequency temperature variability (Ludescher et al., 2020).

The warmest proxy-based summer in the western Mediterranean region is 2017 CE, negating any speculation of a prolonged warming hiatus (Gleisner et al., 2015). It should be further noted that the measured MJJAS temperatures for 2022 (Serrano-Notivoli et al., 2023) clearly exceed any of the reconstructed western Mediterranean summer anomalies since 1119 CE (Figs. 4, 5A). A continuation of the unprecedented recent warming over the 21st century, which is broadly anticipated by climate model simulations (IPCC, 2021), will likely threaten the functioning and productivity of agricultural, ecological, and societal systems in southern Europe and northern Africa (Cramer et al., 2018; Plan Bleu, 2020). The observed long-term warming over the Pyrenees is in line with a similar trend reported from northern Greece (Esper et al., 2020), thought to reflect possible summer insolation changes due to orbital forcing in southern Europe (Laskar et al., 2004). There is also evidence for superimposed cyclic behaviour of our reconstruction at 28 years (not shown), which aligns with analogous periodicities reported from river runoff and flood records (Pekárová et al., 2003; Labat, 2008) possibly related to internal climate variability from ocean-atmosphere couplings. Some of the coldest reconstructed periods coincide with the Wolf, Spörer, Maunder and Dalton solar minima in the second half of the 13th century, around 1490, 1700 and 1810 CE (Fig. 5A), respectively.

Our paleoclimatic findings shed new light on pivotal events in the history of the western Mediterranean region and its larger-scale explorations. We find evidence for a lack of military conflict during or following years with exceptionally hot or cold summers on the Iberian Peninsula. The newly compiled historical evidence further demonstrates generally less warfare and more stable wheat prices during warmer periods. However, caution is advised as any investigation of the human-climate nexus should consider the complex interplay of environmental and societal factors that are difficult to disentangle.

We expect that exploration of additional treeline ecotones in remote parts of the Pyrenees can extend the western Mediterranean summer temperature record further back in time. Moreover, we advocate dendroclimatic research to expand towards the eastern Mediterranean region, where yet unexploited tree-ring archives encounter rich archaeological and historical sources, and where the ecological and societal consequences of anthropogenic climate change call for a precise contextualisation against past natural variation. Finally, we argue that improved climate reconstructions, when carefully integrated with quantitative archaeological and textual records, can improve our understanding of the human past.

Author contributions

U.B. conceived the study, conducted fieldwork, performed the analyses, and wrote the paper. F.R., A.V., A.P., M.To., E.M.D., J.J.C. and J.E. supported fieldwork. A.V. and M.K. measured wood density. P.Sl. and P. St. provided historical and meteorological data and contributed to the analyses. All authors were involved in discussions and helped writing the manuscript.

CRediT authorship contribution statement

Ulf Büntgen: Conceptualization, Data curation, Formal analysis, Funding acquisition, Investigation, Methodology, Project administration, Resources, Supervision, Writing – original draft, Writing – review & editing. **Frederick Reinig:** Investigation, Writing – original draft. **Anne Verstege:** Data curation, Formal analysis. **Alma Piermattei:** Conceptualization, Data curation, Formal analysis. **Marcel Kunz:** Investigation. **Paul Krusic:** Formal analysis, Software, Writing – original draft. **Philip Slavin:** Data curation, Investigation, Methodology, Writing – original draft. **Petr Štěpánek:** Investigation, Methodology. **Max Torbenson:** Methodology, Writing – original draft. **Edurne Martinez del Castillo:** Investigation, Writing – original draft. **Tito Arosio:** Methodology, Software. **Alexander Kirdyanov:** Methodology, Writing – original draft. **Clive Oppenheimer:** Writing – original draft, Writing – review & editing. **Mirek Trnka:** Funding acquisition, Methodology, Project

administration. **Audrey Palosse:** Writing – original draft. **Tatiana Bebchuk:** Software, Writing – original draft. **J. Julio Camarero:** Funding acquisition, Investigation. **Jan Esper:** Conceptualization, Data curation, Formal analysis, Funding acquisition, Writing – original draft, Writing – review & editing.

Declaration of Competing Interest

The authors declare no competing interests.

Data availability

Data will be made available on request.

Acknowledgements

The National Park "Aigüestortes i Estany de Sant Maurici" provided sampling permissions, and Meteo France temperature measurements from Pic du Midi. U.B. and J.E. were supported by the Czech Science Foundation grant HYDRO8 (23-08049S), and the ERC Advanced grant MONOSTAR (AdG 882727). The interdisciplinary aspect of the study was stimulated by the Cooperation Group 'Volcanoes, Climate and History' at the Centre for Interdisciplinary Research (ZiF) in Bielefeld, Germany. Anonymous referees provided useful comments and suggestions.

Appendix A. Supplementary data

Supplementary data to this article can be found online at https://doi.org/10.1016/j.gloplacha.2023.104336.

References

Abulafia, D., 2011. Mediterranean history as global history. History Theory 50, 220–228.
Argilés i Aluja, M.C., 1999. Preus I Salaris a La Lleida Dels Segles XIV I XV Segons Els Llibres D'obra De La Seu. Universitat de Lleida, Lleida.
Barriendos, M., Martín-Vide, J., Peña, J.C., Rodrígues, R., 2002. Daily Meteorological Observations in Cádiz – San Fernando. Analysis of the Documentary sources and the Instrumental Data Content (1786–1996). Clim. Chang. 53, 151–170.
Benito i Monclús, P., 2016. Crisis De Subsistència I Polítiques Frumentàries a La Barcelona Medieval. In: Proveir Barcelona: El Municipi I L'alimentació De La Ciutat. Museu d'Història de Barcelona, Barcelona, pp. 1329–1930.
Björklund, J., Arx, G., Nievergelt, D., Wilson, R., van den Bulcke, J., Günther, B., Loader, N.J., Rydval, M., Fonti, P., Scharnweber, T., Andreu-Hayles, L., Büntgen, U., D'Arrigo, R., Davi, N., De Mil, T., Esper, J., Gärtner, H., Geary, J., Gunnarson, B.E., Hartl, C., Hevia, A., Song, H., Janecka, K., Kaczka, R.J., Kirdyanov, A.V., Kochbeck, M., Liu, Y., Meko, M., Mundo, I., Nicolussi, K., Oelkers, R., Pichler, T., Sánchez-Salguero, R., Schneider, L., Schweingruber, F., Timonen, M., Trouet, V., Van Acker, J., Verstege, A., Villalba, R., Wilmking, M., Frank, D., 2019. Scientific merits and analytical challenges of tree-ring densitometry. Rev. Geophys. 57, 1224–1264.
Briffa, K.R., Jones, P.D., Schweingruber, F.H., 1992. Tree-ring density reconstructions of summer temperature patterns across western North America since 1600. J. Clim. 5, 735–754.
Brogli, R., Lund Sørland, S., Kröner, N., Schär, C., 2021. Future summer warming pattern under climate change is affected by lapse-rate changes. Weather Clim. Dynam. 2, 1093–1110.
Büntgen, U., 2023. Experimental evidence for a thermal limitation of plant cell wall lignification at the alpine treeline. Alp. Bot. 133, 179–182.
Büntgen, U., Oppenheimer, C., 2020. The importance of "year zero" in interdisciplinary studies of climate and history. Proc. Natl. Acad. Sci. U.S.A. 117, 32845–32847.
Büntgen, U., Frank, D.C., Nievergelt, D., Esper, J., 2006. Summer temperature variations in the European Alps, AD 755-2004. J. Clim. 19, 5606–5623.
Büntgen, U., Frank, D., Grudd, H., Esper, J., 2008. Long-term summer temperature variations in the Pyrenees. Clim. Dyn. 31, 615–631.
Büntgen, U., Frank, D., Neuenschwander, T., Esper, J., 2012. Fading temperature sensitivity of alpine tree growth at its Mediterranean margin and associated effects on large-scale climate reconstructions. Clim. Chang. 114, 651–666.
Büntgen, U., Krusic, P.J., Verstege, A., Sangüesa-Barreda, G., Wagner, S., Camarero, J.J., Ljungqvist, F.C., Zorita, E., Oppenheimer, C., Konter, O., Tegel, W., Gärtner, H., Cherubini, P., Reinig, F., Esper, J., 2017. New tree-ring evidence from the pyrenees reveals western Mediterranean climate variability since medieval times. J. Clim. 30, 5295–5318.
Büntgen, U., Arseneault, D., Boucher, É., Churakova (Sidorova), O.V., Gennaretti, F., Crivellaro, A., Hughes, M.K., Kirdyanov, A.V., Klippel, L., Krusic, P.J., Linderholm, H.W., Ljungqvist, F.C., Ludescher, J., McCormick, M., Myglan, V.S., Nicolussi, K., Piermattei, A., Oppenheimer, C., Reinig, F., Sigl, M., Vaganov, E.A., Esper, J., 2020. Prominent role of volcanism in common era climate variability and human history. Dendrochronologia. 64, 125757.
Büntgen, U., Allen, K., Anchukaitis, K.J., Arseneault, D., Boucher, É., Bräuning, A., Chatterjee, S., Cherubini, P., Churakova, O.V., Corona, C., Gennaretti, F., Grießinger, J., Guillet, S., Guiot, J., Gunnarson, B., Helama, S., Hochreuther, P., Hughes, M.K., Huybers, P., Kirdyanov, A.V., Krusic, P.J., Ludescher, J., Meier, W.J.-H., Myglan, V.S., Nicolussi, K., Oppenheimer, C., Reinig, F., Salzer, M.W., Seftigen, K., Stine, A.R., Stoffel, M., St. George, S., Tejedor, E., Trevino, A., Trouet, V., Wang, J., Wilson, R., Yang, B., Xu, G., Esper, J., 2021. The influence of decision-making in tree Ring-based climate reconstructions. Nat. Commun. 12, 3411.
Büntgen, U., Piermattei, A., Crivellaro, A., Reinig, F., Krusic, P.J., Trnka, M., Torbenson, M., Esper, J., 2022a. Common era treeline fluctuations and their implications for climate reconstructions. Glob. Planet. Chang. 219, 103979.
Büntgen, U., Piermattei, A., Krusic, P.J., Esper, J., Sparks, T., Crivellaro, A., 2022b. Plants in the UK flower a month earlier under recent warming. Proc. R. Soc. B Biol. Sci. 289, 202124562.
Büntgen, U., Hodgson Smith, S., Wagner, S., Krusic, P., Esper, J., Piermattei, A., Crivellaro, A., Reinig, F., Tegel, W., Kirdyanov, A., Trnka, M., Oppenheimer, C., 2022c. Global tree-ring response and inferred climate variation following the mid-thirteenth century Samalas eruption. Clim. Dyn. 59, 531–546.
Camarero, J.J., Gazol, A., Sánchez-Salguero, R., Fajardo, A., McIntire, E.J., Gutiérrez, E., Batllori, E., Boudreau, S., Carrer, M., Diez, J., Dufour-Tremblay, G., Gaire, N.P., Hofgaard, A., Jomelli, V., Kirdyanov, A.V., Lévesque, E., Liang, E., Linares, J.C., Mathisen, I.E., Moiseev, P.A., Sangüesa-Barreda, G., Shrestha, K.B., Toivonen, J.M., Tutubalina, O.V., Wilmking, M., 2021. Global fading of the temperature–growth coupling at Alpine and polar treelines. Glob. Chang. Biol. 27, 1879–1889.
Carreras, A., Tafunell, X., 2005. Estadísticas Históricas de España: Siglos XIX-XX. BBVA, Bilbao.
Catlos, B., 2018. Kingdoms of Faith: A New History of Islamic Spain. Basic Books, New York.
Chree, C., 1913. Some phenomena of sunspots and of terrestrial magnetism at Kew Observatory. Phil. Trans. R. Soc. Lond. Ser. A Contain. Pap. Math. Phys. Charac. 212, 75–116.
Cook, E.R., Peters, K., 1981. The smoothing spline: a new approach to standardizing forest interior tree-ring width series for dendroclimatic studies. Tree-Ring Bull. 41, 45–53.
Cook, E.R., Peters, K., 1997. Calculating unbiased tree-ring indices for the study of climatic and environmental change. The Holocene 7, 361–370.
Cook, E.R., Briffa, K.R., Meko, D.M., Graybill, D.A., Funkhouser, G., 1995. The "segment length curse" in Long Tree-ring chronology development for Palaeoclimatic Studies. The Holocene 5, 229–237.
Cook, E.R., Meko, D.M., Stahle, D.W., Cleaveland, M.K., 1999. Drought reconstructions for the continental United States. J. Clim. 12, 1145–1162.
Cook, E.R., Krusic, P.J., Peters, K., Holmes, R.L., 2005. Program ARSTAN Autoregressive Tree–Ring Standardization Program. Tree–Ring Laboratory of Lamont–Doherty Earth Observatory.
Cook, E.R., Seager, R., Kushnir, Y., Briffa, K.R., Büntgen, U., Frank, D., Krusic, P.J., Tegel, W., van der Schrier, G., Andreu-Hayles, L., Baillie, M., Baittinger, C., Bleicher, N., Bonde, N., Brown, D., Carrer, M., Cooper, R., Čufar, K., Dittmar, C., Esper, J., Griggs, C., Gunnarson, B., Günther, B., Gutierrez, E., Haneca, K., Helama, S., Herzig, F., Heussner, K.-U., Hofmann, J., Janda, P., Kontic, R., Köse, N., Kyncl, T., Levanič, T., Linderholm, H., Manning, S., Melvin, T.M., Miles, D., Neuwirth, B., Nicolussi, K., Nola, P., Panayotov, M., Popa, I., Rothe, A., Seftigen, K., Seim, A., Svarva, H., Svoboda, M., Thun, T., Timonen, M., Touchan, R., Trotsiuk, V., Trouet, V., Walder, F., Ważny, T., Wilson, R., Zang, C., 2015. Old world megadroughts and pluvials during the common era. Sci. Adv. 1, e1500561.
Cornes, R., van der Schrier, G., van den Besselaar, E., Jones, P., 2018. An ensemble version of the E-OBS temperature and precipitation data sets. J. Geophys. Res.-Atmos. 123, 9391–9409.
Cramer, W., Guiot, J., Fader, M., Garrabou, J., Gattuso, J.-P., Iglesias, A., Lange, M.A., Lionello, P., Llasat, M.C., Paz, S., Peñuelas, J., Snoussi, M., Toreti, A., Tsimplis, M.N., Xoplaki, E., 2018. Climate change and interconnected risks to sustainable development in the Mediterranean. Nat. Clim. Chang. 8, 972–980.
Dessens, J., Bücher, A., 1995. Changes in minimum and maximum temperatures at the Pic du Midi in relation with humidity and cloudiness, 1882-1984. Atmos. Res. 37, 147–162.
Di Cosmo, N., Oppenheimer, C., Büntgen, U., 2017. Interplay of environmental and socio-political factors in the downfall of the Eastern Türk Empire in 630 CE. Clim. Chang. 145, 383–395.
Durbin, J., Watson, G.S., 1951. Testing for serial correlation in least squares regression. Biometrika. 38, 159–177.
Eschbach, W., Nogler, P., Schaer, E., Schweingruber, F.H., 1995. Technical advances in the radiodensitometrical determination of wood density. Dendrochronologia. 12, 155–168.
Esper, J., Cook, E.R., Krusic, P.J., Peters, K., Schwingruber, F.H., 2003. Tests of the RCS method for preserving low-frequency variability in long tree-ring chronologies. Tree-Ring Res. 59, 81–98.
Esper, J., Frank, D.C., Wilson, R.J.S., Briffa, K.R., 2005. Effect of scaling and regression on reconstructed temperature amplitude for the past millennium. Geophys. Res. Lett. 32, L07711.
Esper, J., Frank, D.C., Timonen, M., Zorita, E., Wilson, R.J.S., Luterbacher, J., Holzkämper, S., Nievergelt, D., Verstege, A., Büntgen, U., 2012. Orbital forcing of tree-ring data. Nat. Clim. Chang. 2, 862–866.
Esper, J., Schneider, L., Krusic, P.J., Luterbacher, J., Büntgen, U., Timonen, M., Sirocko, F., Zorita, E., 2013. European summer temperature response to annually dated volcanic eruptions over the past nine centuries. Bull. Volcanol. 75, 736–750.

Esper, J., Krusic, P.J., Ljungqvist, F.C., Luterbacher, J., Carrer, M., Cook, E., Davi, N.K., Hartl-Meier, C., Kirdyanov, A., Konter, O., Myglan, V., Timonen, M., Treydte, K., Trouet, V., Villalba, R., Yang, B., Büntgen, U., 2016. Ranking of tree-ring based temperature reconstructions of the past Millennium. Quat. Sci. Rev. 145, 134–151.
Esper, J., Büntgen, U., Denzer, S., Krusic, P.J., Luterbacher, J., Schäfer, R., Schreg, R., Werner, J., 2017a. Environmental drivers of historical grain price variations in Europe. Clim. Res. 72, 39–52.
Esper, J., Büntgen, U., Hartl-Meier, C., Oppenheimer, C., Schneider, L., 2017b. Northern Hemisphere temperature anomalies during the 1450s period of ambiguous volcanic forcing. Bull. Volcanol. 79, 41.
Esper, J., Klippel, L., Krusic, P.J., Konter, O., Raible, C.C., Xoplaki, E., Luterbacher, J., Büntgen, U., 2020. Eastern Mediterranean summer temperatures since 730 CE from Mt. Smolikas tree-ring densities. Clim. Dyn. 54, 1367–1382.
Essell, H., Krusic, J., Esper, J., Wagner, S., Braconnot, P., Jungclaus, J., Muschitiello, F., Oppenheimer, C., Büntgen, U., 2023. A frequency-optimised temperature record for the Holocene. Environ. Res. Lett. 18, 114022.
Feliu, G., 1991. Precios y Salarios en la Cataluña Moderna. Banco de España, Madrid.
Fischer, E.M., Knutti, R., 2015. Anthropogenic contribution to global occurrence of heavy-precipitation and high-temperature extremes. Nat. Clim. Chang. 5, 560–564.
Frank, D., Esper, J., Cook, E.R., 2007a. Adjustment for proxy number and coherence in a large-scale temperature reconstruction. Geophys. Res. Lett. 34, L1670.
Frank, D.C., Büntgen, U., Böhm, R., Maugeri, M., Esper, J., 2007b. Warmer early instrumental measurements versus colder reconstructed temperatures: shooting at a moving target. Quat. Sci. Rev. 26, 3298–3310.
Franklin-Lyons, A., 2009. Famine – Preparation and Response in Catalonia after the Black Death. Yale University, New Haven CT.
Franklin-Lyons, A., 2022. Shortage and Famine in the Late Medieval Crown of Aragon. Pennsylvania State University Press, University Park, PA.
Fritts, H., 1976. Tree Rings and Climate. Academic Press, New York.
Galván, J.D., Camarero, J.J., Ginzler, C., Büntgen, U., 2014. Spatial diversity of recent trends in Mediterranean Tree Growth. Environ. Res. Lett. 9, 084001.
García Fitz, F., Gouveia Monteiro, J., 2018. War in the Iberian Peninsula, 700–1600. Routledge, Abingdon.
Giorgi, F., 2006. Climate change hot-spots. Geophys. Res. Lett. 33, L08707.
Gleisner, H., Thejll, P., Christiansen, B., Nielsen, J.K., 2015. Recent global warming hiatus dominated by low-latitude temperature trends in surface and troposphere data. Geophys. Res. Lett. 42, 510–517.
Glete, J., 2001. War and the State in Early Modern Europe: Spain, the Dutch Republic and Sweden as Fiscal-Military States. Routledge, London.
Guillet, S., Corona, C., Oppenheimer, C., Lavigne, F., Khodri, M., Ludlow, F., Sigl, M., Toohey, M., Atkins, P.S., Yang, Z., Muranaka, T., Horikawa, N., Stoffel, M., 2023. Lunar eclipses illuminate timing and climate impact of medieval volcanism. Nature. 616, 90–95.
Harris, I., Osborn, T.J., Jones, P., Lister, D., 2020. Version 4 of the Cru Ts monthly high-resolution gridded Multivariate Climate Dataset. Sci. Data 7, 109.
IPCC, 2021. Climate change 2021: The physical science basis. In: Masson-Delmotte, V.P., Zhai, A., Pirani, S.L., Connors, C., Péan, S., Berger, S.N., et al. (Eds.), Contribution of Working Group I to the Sixth Assessment Report of the Intergovernmental Panel on Climate Change. Cambridge University Press, Cambridge, UK.
Jacks, D., 2006. Intra- and International Commodity Market Integration in the Atlantic Economy, 1800-1913. Explor. Econ. Hist. 42, 381–413.
Jones, P.D., Moberg, A., 2003. Hemispheric and large-scale surface air temperature variations: an extensive revision and an update to 2001. J. Clim. 16, 206–223.
Kamen, H., 2005. Spain, 1469–1714. A Society of Conflict, Pearson, Harlow.
Kelley, C.P., Mohtadi, S., Cane, M.A., Seager, R., Kushnir, Y., 2015. Climate change in the Fertile Crescent and implications of the recent Syrian drought. Proc. Natl. Acad. Sci. U.S.A. 112, 3241–3246.
Klein Tank, A.M., Wijngaard, J.B., Können, G.P., Böhm, R., Demarée, G., Gocheva, A., Mileta, M., Pashiardis, S., Hejkrlik, L., Kern-Hansen, C., Heino, R., Bessemoulin, P., Müller-Westermeier, G., Tzanakou, M., Szalai, S., Pálsdóttir, T., Fitzgerald, D., Rubin, S., Capaldo, M., Maugeri, M., Leitass, A., Bukantis, A., Aberfeld, R., van Engelen, A.F., Forland, E., Mietus, M., Coelho, F., Mares, C., Razuvaev, V., Nieplova, E., Cegnar, T., Antonio López, J., Dahlström, B., Moberg, A., Kirchhofer, W., Ceylan, A., Pachaliuk, O., Alexander, L.V., Petrovic, P., 2002. Daily dataset of 20th-century surface air temperature and precipitation series for the European climate Assessment. Int. J. Climatol. 22, 1441–1453.
Körner, C., Lenz, A., Hoch, G., 2023. Chronic in situ tissue cooling does not reduce lignification at the Swiss treeline but enhances the risk of 'blue' frost rings. Alp. Bot. 133, 63–67.
Labat, D., 2008. Wavelet analysis of the annual discharge records of the world's largest rivers. Adv. Water Resour. 31, 109–117.
Laskar, J., Robutel, P., Joutel, F., Gastineau, M., Correia, A.C.M., Levrard, B., 2004. A long-term numerical solution for the insolation quantities of the Earth. Astron. Astrophys. 428, 261–285.
Lavigne, F., Degeai, J.-P., Komorowski, J.-C., Guillet, S., Robert, V., Lahitte, P., Oppenheimer, C., Stoffel, M., Vidal, C.M., Pratomo, S.I., Wassmer, P., Hajdas, I., Hadmoko, D.S., de Belizal, E., 2013. Source of the great AD 1257 mystery eruption unveiled, Samalas volcano, Rinjani Volcanic Complex, Indonesia. Proc. Natl. Acad. Sci. U.S.A. 110, 16742–16747.
Ljungqvist, F.C., Piermattei, A., Seim, A., Krusic, P.J., Büntgen, U., He, M., Kirdyanov, A. V., Luterbacher, J., Schneider, L., Seftigen, K., Stahle, D.W., Villalba, R., Yang, B., Esper, J., 2020. Ranking of tree-ring based hydroclimate reconstructions of the past Millennium. Quat. Sci. Rev. 230, 106074.
Ljungqvist, F.C., Seim, A., Collet, D., 2023. Famines in medieval and early modern Europe – connecting climate and society. WIREs Clim. Change, e859.
Lomax, D.W., 1978. The Reconquest of Spain. Longman, London.
Ludescher, J., Bunde, A., Büntgen, U., Schellnhuber, H.J., 2020. Setting the tree-ring record straight. Clim. Dyn. 3, 3017–3024.
Luterbacher, J., et al., 2012. A review of 2000 years of paleoclimatic evidence in the Mediterranean. In: Lionello, P. (Ed.), The Climate of the Mediterranean Region: From the Past to the Future. Elsevier, Amsterdam, The Netherlands, pp. 87–185.
Maltas i Montoro, J., 2019. Caresties, Fams I Crisis de Mortalitat a Catalunya: 1283–1351. Universitat de Lleida, Lleida.
McCormick, M., Büntgen, U., Cane, M.A., Cook, E.R., Harper, K., Huybers, P., Litt, T., Manning, S.W., Mayewski, P.A., More, A.F.M., Nicolussi, K., Tegel, W., 2012. Climate change during and after the Roman Empire: reconstructing the past from scientific and historical evidence. J. Interdiscip. Hist. XLIII, 169–220.
Medhaug, I., Stolpe, M.B., Fischer, E.M., Knutti, R., 2017. Reconciling controversies about the global warming hiatus. Nature. 545, 41–47.
O'Callaghan, J.F., 2003. Reconquest and Crusade in Medieval Spain. University of Pennsylvania Press, Philadelphia.
O'Callaghan, J.F., 2014. The Last Crusade in the West: Castile and the Conquest of Granada. University of Pennsylvania Press, Philadelphia.
Oppenheimer, C., 2003. Ice Core and palaeoclimatic evidence for the timing and nature of the great mid-13th century volcanic eruption. Int. J. Climatol. 23, 417–426.
Osborn, T.J., Briffa, K.R., Jones, P.D., 1997. Adjusting variance for sample-size in tree-ring chronologies and other regional mean time Series. Dendrochronologia. 15, 89–99.
PAGES2k Consortium, 2019. Consistent multidecadal variability in global temperature reconstructions and simulations over the Common Era. Nat. Geosci. 12, 643–649.
Pekárová, P., Miklánek, P., Pekár, L., 2003. Spatial and temporal runoff oscillation analysis of the main rivers of the world during the 19th–20th centuries. J. Hydrol. 274, 62–79.
Percival, D.B., Walden, A.T., 1993. Spectral Analysis for Physical Applications: Multitaper and Conventional Univariate Techniques. Cambridge University Press, Cambridge.
Piermattei, A., Crivellaro, A., Krusic, P.J., Esper, J., Vítek, P., Oppenheimer, C., Felhofer, M., Gierlinger, N., Reinig, F., Urban, O., Verstege, A., Lobo, H., Büntgen, U., 2020. A millennium-long 'blue ring' chronology from the Spanish Pyrenees reveals severe ephemeral summer cooling after volcanic eruptions. Environ. Res. Lett. 15, 124016.
Plan Bleu, 2020. State of the Environment and Development in the Mediterranean. United Nations Environment Programme/Mediterranean Action Plan and Plan Bleu, SoED, Nairobi.
Reilly, B., 1993. The Medieval Spains. Cambridge University Press, Cambridge.
Rohde, R.A., Hausfather, Z., 2020. The Berkeley Earth Land/Ocean temperature record. Earth Syst. Sci. Data 12, 3469–3479.
Rousi, E., Kornhuber, K., Beobide-Arsuaga, G., Luo, F., Coumou, D., 2022. Accelerated Western European heatwave trends linked to more-persistent double jets over Eurasia. Nat. Commun. 13, 3851.
Schneider, L., Smerdon, J.E., Büntgen, U., Wilson, R.J., Myglan, V.S., Kirdyanov, A.V., Esper, J., 2015. Revising midlatitude summer temperatures back to AD 600 based on a wood density network. Geophys. Res. Lett. 42, 4556–4562.
Schneider, L., Smerdon, J.E., Pretis, F., Hartl-Meier, C., Esper, J., 2017. A new archive of large volcanic events over the past millennium derived from reconstructed summer temperatures. Environ. Res. Lett. 12, 094005.
Schweingruber, F.H., Fritts, H.C., Bräker, O.U., Drew, L.G., Schär, E., 1978. The X-ray technique as applied to dendroclimatology. Tree-Ring Bull. 38, 61–91.
Seager, R., Liu, H., Henderson, N., Simpson, I., Kelley, C., Shaw, T., Kushnir, Y., Ting, M., 2014. Causes of increasing aridification of the Mediterranean region in response to rising greenhouse gases. J. Clim. 27, 4655–4676.
Serrano-Notivoli, R., Tejedor, E., Sarricolea, P., Meseguer-Ruiz, O., de Luis, M., Angel Saz, M., Alberto Longares, L., Olcina, J., 2023. Unprecedented warmth: a look at Spain's exceptional summer of 2022. Atmos. Res. 293, 106931.
Sigl, M., Winstrup, M., McConnell, J.R., Welten, K.C., Plunkett, G., Ludlow, F., Büntgen, U., Caffee, M., Chellman, N., Dahl-Jensen, D., Fischer, H., Kipfstuhl, S., Kostick, C., Maselli, O.J., Mekhaldi, F., Mulvaney, R., Muscheler, R., Pasteris, D.R., Pilcher, J.R., Salzer, M., Schüpbach, S., Steffensen, J.P., Vinther, B.M., Woodruff, T. E., 2015. Timing and climate forcing of volcanic eruptions for the past 2,500 years. Nature. 523, 543–549.
Sigl, M., Toohey, M., McConnell, J.R., Cole-Dai, J., Severi, M., 2022. Volcanic stratospheric sulfur injections and aerosol optical depth during the Holocene (past 11 500 years) from a bipolar ice-core array. Earth Syst. Sci. Data 14, 3167–3196.
Slavin, P., 2016. Climate and famines: a historical reassessment. WIREs Clim. Change. 7, 433–447.
Slavin, P., 2019. Experiencing Famine in Fourteenth-Century Britain. Brepols, Turnhout.
Štěpánek, P., Zahradníček, P., Huth, R., 2011. Interpolation techniques used for data quality control and calculation of technical series: an example of central European daily time series. Időjárás. 115, 87–98.
Štěpánek, P., Zahradníček, P., Farda, A., 2013. Experiences with data quality control and homogenization of daily records of various meteorological elements in the Czech Republic in the period 1961–2010. Időjárás. 117, 123–141.
Stoffel, M., Khodri, M., Corona, C., Guillet, S., Poulain, V., Bekki, S., Luckman, B.H., Oppenheimer, C., Lebas, N., Beniston, M., Masson-Delmotte, V., 2015. Estimates of volcanic-induced cooling in the Northern Hemisphere over the past 1,500 years. Nat. Geosci. 8, 784–788.
Tegel, W., Muigg, B., Skiadaresis, G., Vanmoerkerke, J., Seim, A., 2022. Dendroarchaeology in Europe. Front. Ecol. Evol. 10, 823622.
Torbenson, M.C.A., Plunkett, G., Brown, D.M., Pilcher, J.R., Leuschner, H.-H., 2015. Asynchrony in key Holocene chronologies: evidence from Irish bog pines. Geology. 43, 799–803.

Touchan, R., Anchukaitis, K.J., Meko, D.M., Kerchouche, D., Slimani, S., Ilmen, R., Hasnaoui, F., Guibal, F., Camarero, J.J., Sánchez-Salguero, R., Piermattei, A., Sesbou, A., Cook, I., Sabir, M., Touchane, H., 2017. Climate controls on tree growth in the Western Mediterranean. The Holocene 27, 1429–1442.
Trapletti, A., Hornik, K., LeBaron, B., 2023. Package 'tseries' (R) v.0.10–54.
Wigley, T.M.L., Briffa, K.R., Jones, P.D., 1984. On the average value of correlated time series, with applications in dendroclimatology and hydrometeorology. Am. Meteorol. Soc. 23, 201–213.
Wunderling, N., Winkelmann, R., Rockström, J., Loriani, S., Armstrong McKay, D.I., Ritchie, P.D., Sakschewski, B., Donges, J.F., 2023. Global warming overshoots increase risks of climate tipping cascades in a network model. Nat. Clim. Chang. 13, 75–82.